Inorg. Chem. **2005**, *44*, 6192–6196

Open Metal–Organic Framework Containing Cuprate Chains

Dat T. Tran,[†] Xiaojuan Fan,[†] Daniel P. Brennan,[†] Peter Y. Zavalij,[‡] and Scott R. J. Oliver*,[†]

Department of Chemistry and Biochemistry, University of California, Santa Cruz, 1156 High Street, Santa Cruz, California 95064, and Institute for Materials Research, State University of New York at Binghamton, Binghamton, New York 13902-6000

Received January 7, 2005

A three-dimensional Cu(II) metal–organic framework, copper hydroxide *p*-pyridinecarboxylate hydrate, $[Cu(OH)(C_5H_4NCO_2)\cdot H_2O]$, was synthesized by hydrothermally reacting copper nitrate with *p*-pyridinecarboxylic acid. The crystals were suitable for single-crystal X-ray diffraction analysis, which showed that the Cu(II) centers adopt a slightly distorted square pyramidal geometry. They coordinate to both the pyridyl and carboxylate functionalities of the pyridinecarboxylate bridging ligands. Infinite copper oxide chains run through the structure and are connected by *p*-pyridinecarboxylate (*p*-PyC) ligands. Crystal data: monoclinic, space group $P2_1/n$, $a = 3.5521(2)$ Å, $b = 15.8665(11)$ Å, $c = 12.9977(9)$ Å, $\beta = 95.285(2)°$, and $Z = 4$. Thermogravimetric analysis (TGA) revealed that the guest H_2O molecules in the channels may be removed, and the material is stable to ca. 245 °C. Magnetic measurements indicated the material has one-dimensional (1D) antiferromagnetic ordering within the Cu^{2+} chains with a Néel temperature of ca. 51 K. Data fitting to the Bonner–Fisher model yielded a coupling constant, *J*, of -7.3 cm^{-1} and *g* factor of 2.15. The Curie tail below 20 K is due to a small amount of paramagnetic impurities, calculated to be ~0.2% in concentration. Further characterization of crystallinity and morphology are discussed, including powder X-ray diffraction (PXRD), elemental analysis, and optical microscopy.

Introduction

In recent years the synthesis of new metal−organic coordination compounds has received increasing interest.[1−14] These extended architectures contain metal ions coordinated by organic ligands to produce porous coordination frameworks. The guest species in the open channels can often be removed and reintroduced reversibly without destroying the framework.[13] Potential applications of these materials include second-order nonlinear optical activity,[7] gas adsorption,[8a] hydrogen storage,[8b] guest exchange,[8c] and selective catalysis.[9,10] Main-group and transition metals are the most commonly investigated, with coordination numbers of four to six. Actinide and lanthanide elements, however, allow metal−organic frameworks with metal coordination numbers greater than seven.[11−14]

Much effort has been placed on the design of porous materials with new pore functionalities that are also

* To whom correspondence should be addressed. E-mail: soliver@chemistry.ucsc.edu. Phone: (831) 459-5448. Fax: (831) 459-2935.
[†] University of California, Santa Cruz.
[‡] State University of New York at Binghamton.

(1) See, for example: (a) Cheetham, A. K.; Férey, G.; Loiseau, T. *Angew. Chem., Int. Ed.* **1999**, *38*, 3268−3292. (b) Rao, C. N. R.; Natarajan, S.; Vaidhyanathan, R. *Angew. Chem., Int. Ed.* **2004**, *43*, 1466−1496.
(2) (a) Bu, X.; Tong, M.; Chang, H.; Kitagawa, S.; Batten, S. R. *Angew. Chem., Int. Ed.* **2004**, *43*, 192−195. (b) Blake, A. J.; Champness, N. R.; Hubberstey, P.; Li, W.-S.; Withersby, M. A.; Schroder, M. *Coord. Chem. Rev.* **1999**, *183*, 117−138.
(3) Robson, R. *Dalton Trans.* **2000**, 3735−3744.
(4) Eddaoudi, M.; Moler, D. B.; Li, H.; Chen, B.; Reineke, T. M.; O'Keeffe, M.; Yaghi, O. M. *Acc. Chem. Res.* **2001**, *34*, 319−330.
(5) Moulton, B.; Zaworotko, M. J. *Chem. Rev.* **2001**, *101*, 1629−1658.
(6) Hollingsworth, M. D. *Science* **2002**, *295*, 2410−2413.
(7) (a) Lin, W.; Evans, O. R.; Xiong, R.-G.; Wang, Z. *J. Am. Chem. Soc.* **1998**, *120*, 13272−13273. (b) Lin, W.; Wang, Z.; Ma, L. *J. Am. Chem. Soc.* **1999**, *121*, 11249−11250. (c) Lin, W.; Ma, L.; Evans, O. R. *Chem. Commun.* **2000**, *22*, 2263−2264.
(8) (a) Eddaoudi, M.; Kim, J.; Rossi, N.; Vodak, D.; Wachter, J.; O'Keeffe, M.; Yaghi, O. M. *Science* **2002**, *295*, 469−472. (b) Rosi, N. L.; Eckert, J.; Eddaoudi, M.; Vodak, D. T.; Kim, J.; O'Keeffe, M.; Yaghi, O. M. *Science* **2003**, *300*, 1127−1129. (c) Chae, H. K.; Siberio-Perez, D. Y.; Kim, J.; Go, Y.; Eddaoudi, M.; Matzger, A. J.; O'Keeffe, M.; Yaghi, O. M. *Nature* **1995**, *378*, 703−706.
(9) Fujita, M.; Kwon, Y. J.; Washzu, S.; Ogura, K. *J. Am. Chem. Soc.* **1994**, *116*, 1151−1152.
(10) Chae, H. K.; Siberio-Perez, D. Y.; Kim, J.; Go Y.; Eddaoudi, M.; Matzger, A. J.; O'Keeffe, M.; Yaghi, O. M. *Nature* **2004**, *427*, 523−527.
(11) (a) Serpaggi, F.; Férey, G. *J. Mater. Chem.* **1998**, *8*, 2737−2741. (b) Kim, J.-Y.; Norquist, A. J.; O'Hare, D. *J. Am. Chem. Soc.* **2003**, *125*, 12688−12689.
(12) Ciurtin, D. M.; Smith, M. D.; zur Loye, H.-C. *Inorg. Chim. Acta.* **2001**, *324*, 46−56.
(13) Pan, L.; Adams, K. M.; Hernandez, H. E.; Wang, X.; Zheng, C.; Hattori, Y.; Kaneko, K. *J. Am. Chem. Soc.* **2003**, *125*, 3062−3067.
(14) Finn, R. C.; Burkholder, E.; Zubieta, J. In Crystal Design: Structure and Function. *Perspectives in Supramolecular Chemistry*; Desiraju, G. R., Ed.; Wiley & Sons: Chichester, 2003; Vol. 7, pp 241−274.

10.1021/ic050024c CCC: $30.25
Published on Web 08/12/2005

accessible.[15−17] Exploitation of the micropores within such crystal structures has been the main focus. One recent example is a homochiral metal−organic porous material that exhibits enantioselective separation and catalysis.[18] Another example is a microporous material displaying high framework stability and highly selective gas sorption properties.[19] In addition to the work of Yaghi and co-workers, Rosseinsky and co-workers showed that the design of nanoporous MOFs can be useful for creating H_2 storage materials.[20a]

Despite this rich chemistry, metal−organic structures with extended inorganic chains embedded within the structure are very uncommon. To our knowledge, there exist only several such examples to date. Two are based on nine-coordinate metals, namely, neodymium oxide hydrate[11a] or thorium oxyfluoride[11b] chains. Another contains alternating copper(I) and chloride with these chains running through the framework.[12] Their report also describes a related structure containing copper(I) bromide layers. In addition, Férey and co-workers reported two copper diphosphonates that both show antiferromagnetic behavior.[20b] They also reported a series of four structures in the NaOH−Cu−phosphonate system whose magnetic properties depend on the structure type.[20c]

Hydroxo-bridged copper(II) systems[21a] often display a spin dimer motif, and their magnetic properties have been studied extensively. Magnetic studies of 1D chain structures have also been reported. Hiller et al.[21b] described a metal−organic alternating spin chain system $[FeON_8C_{26}H_{14}]_n$, where the Fe ions are antiferromagnetically coupled. Hatfield and co-workers also reported magnetic susceptibility and structural data for sulfur-bridged[21c] and halide-bridged[21d] linear chain copper organohalide compounds. The coupling exchange between metal centers in these systems is in the range from ca. -6.7 to -22.3 cm^{-1}, as determined using the Heisenberg chain theory of Bonner and Fisher.[22]

Zigzag Cu (II) oxide spin ladder chains present in the title compound, however, have not been previously reported. The theoretical 1D Heisenberg chain model may be applied to susceptibility−temperature data to deduce the exchange interaction between the oxygen-bridged Cu ions. Here, we report the first of a series of new metal−organic materials, a 3D metal−organic open framework, **1,** with infinite 1D Cu(II) oxide chains embedded in the structure. The crystal structure, thermal properties, and magnetic properties with data fitting to theoretical models are described.

Experimental Section

Synthetic Procedure. Copper hydroxide *p*-pyridinecarboxylate (*p*-PyC) hydrate $[Cu(OH)(C_5H_4NCO_2)\cdot H_2O]$, **1**, was synthesized in a simple, one-step reaction. The following reagents were added as-received to a 250 mL Nalgene beaker with thorough manual mixing after each step: (i) distilled water; (ii) $Cu(NO_3)_2\cdot 3H_2O$ (Fisher); (iii) 4-pyridinecarboxylic acid (*p*-PyCH, Acros, 99%). The molar ratio was 250:1:1, respectively, and the mixture was stirred mechanically for about 15 min. A 23 mL capacity Teflon-lined Parr autoclave was filled to approximately two-thirds capacity and heated at 150 °C for 4 days. The needle-shaped, dark blue-green crystals were suction filtered, rinsed with distilled water, and allowed to dry with a typical yield of 65%. Elemental analysis (Quantitative Technologies Inc., Whitehouse, NJ) of the as-synthesized product (31.76% C, 2.75% H, 6.06% N) also agrees well with the theoretical values based on the stoichiometric formula $H_7C_6NO_4Cu$ (32.63% C, 3.17% H, 6.34% N).

Characterization Methods. Powder X-ray diffraction (PXRD) was carried out with a Scintag XDS 2000 powder diffractometer using Cu Kα radiation ($\lambda = 1.5418$ Å), solid-state detector (which removes white radiation and β lines), scan range from 2° to 50° (2θ), step size 0.02°, and scan rate 4.0°/min. Samples were ground thoroughly in a mortar and pestle prior to mounting the resultant powder in the PXRD sample holder; TGA was carried out with a TA Instruments 2950 using a 5 °C/min scan rate and nitrogen purge; optical microscopy was collected on a Nikon Inverted Metallurgical Microscope, Model Epiphot 200, equipped with a digital high-resolution CCD camera and integrated image processing (Image-Pro Plus software); SQUID magnetometry: Quantum Design, MPMS, where the DC Magnetization was registered in field-cooling condition at an applied magnetic field of 1000 G.

X-ray Crystallography. The crystals were suitable for single-crystal X-ray diffraction analysis. Data for a manually selected crystal was collected on a three-circle diffractometer system equipped with Bruker SmartApex CCD area detector, using a graphite monochromator and a Mo Kα fine-focus sealed tube ($\lambda = 0.710\,73$ Å). Operating conditions were 50 kV and 40 mA, ω-scan, ω step size 0.30°, and 10 s exposition time. The detector was placed at a distance of 5.17 cm from the crystal. The total data collection time was 7.01 h.

Absorption correction was performed with TWINABS software.[23a] The structure was solved and refined using the SHELXS-97[23b] and SHELXL-97[23c] software using data collected from the twinned crystal. The final anisotropic full-matrix least-squares refinement on F^2 with 139 variables converged at $R_1 = 4.05\%$ for the observed data and w$R_2 = 9.50\%$ for all data.

Results and Discussion

Scheme 1 shows the optimal synthetic conditions for **1**, $Cu(OH)(p\text{-PyC})\cdot H_2O$. The ideal synthesis temperature was 150 °C: no solid phase was observed at 125 °C, while 175 °C yielded a mixture of **1** and a dark black solid. The latter

(15) Gardner, G. B.; Kiang, Y.-H.; Lee, S.; Asgaonkar, A.; Venkataraman, D. *J. Am. Chem. Soc.* **1996**, *118*, 6946−6953.
(16) Kiang, Y.-H.; Gardner, G. B.; Lee, S.; Xu, Z.; Lobkovsky, E. B. *J. Am. Chem. Soc.* **1999**, *121*, 8204−8215.
(17) Chui, S. S.-Y.; Lo, S. M.-F.; Charmant, J. P. H.; Orpen, A. G.; Williams, I. D. *Science* **1999**, *283*, 1148−1150.
(18) Seo, J. S.; Whang, D.; Lee, H.; Jun, S. I.; Oh, J.; Jeon, Y. J.; Kim, K. *Nature* **2000**, *404*, 982−986.
(19) Dybtsev, D. N.; Chun, H.; Yoon, S. H.; Kim, D.; Kim, K. *J. Am. Chem. Soc.* **2004**, *126*, 32−33.
(20) (a) Zhao, X.; Xiao, B.; Fletcher, A. J.; Thomas, K. M.; Bradshaw, D.; Rosseinsky, M. J. *Science* **2004**, *306*, 1012−1015. (b) Riou, D.; Belier, F.; Serre, C.; Nogues, M.; Vichard, D.; Férey, G. *Int. J. Inorg. Mater.* **2000**, *2*, 29−33. (c) Barthelet, K.; Nogues, M.; Riou, D.; Férey, G. *Chem. Mater.* **2002**, *14*, 4910−4918.
(21) (a) Crawford, V. H.; Richardson, H. W.; Wasson, J. R.; Hodgson, D. J.; Hatfield, W. E. *Inorg. Chem.* **1976**, *15*, 2107−2110. (b) Hiller, W.; Strähle, J.; Datz, A.; Hanack, M.; Hatfield, W. E.; Haar, L. W.; Gütlich, P. *J. Am. Chem. Soc.* **1984**, *106*, 329−335. (c) Hatfield, W. E.; Weller, R. R.; Hall, J. W. *Inorg. Chem.* **1980**, *19*, 3825−3838. (d) Crawford, V. H.; Hatfield, W. E. *Inorg. Chem.* **1977**, *16*, 1336−1341.
(22) Bonner, J. C.; Fisher, M. E. *Phys. Rev. A* **1964**, *135*, 640−658.
(23) (a) Sheldrick, G. M. *SADABS*; University of Göttingen: Göttingen, Germany, 1996. (b) Sheldrick, G. M. *Acta Crystallogr.* **1990**, *A46*, 467−473. (c) Sheldrick, G. M. *SHELXL-97*; University of Göttingen: Göttingen, Germany, 1997.

Scheme 1. Hydrothermal Reaction of Copper Nitrate Hydrate and *p*-Pyridinecarboxylic Acid Gives Rise to the Extended Metal−Organic Framework

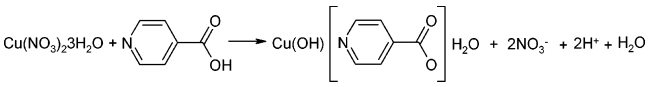

was the only product at 200 °C, likely due to the decomposition of the ligand. The optical micrograph shows the needlelike morphology of the 150 °C product (Figure 1). The product is highly crystalline and phase-pure (Figure 2a), comparing the experimental PXRD pattern to the theoretical pattern based on the single-crystal data (Figure 2b). The patterns agree very well over the entire range. Some higher angle peaks are likely suppressed in the experimental pattern due to preferred orientation upon sample preparation from the needle morphology of the product.

Table 1 displays detailed crystallographic information for the compound. In this structure each Cu atom is coordinated to the oxygens of three hydroxyl groups. Each O atom is coordinated to three Cu atoms to form a zigzag chain of edge-sharing four-rings along the *a*-axis (Figure 3a). In addition, each Cu atom is coordinated by the N atom and one of the two carboxylate oxygens of the *p*-PyC ligand, defining square pyramidal geometry (Table 2). One of the hydroxyl oxygens in the apex of the pyramid resides at an elongated distance

Figure 1. Optical micrograph of **1**, showing the needlelike morphology of the blue-green crystals (white scale bar: 50 μm).

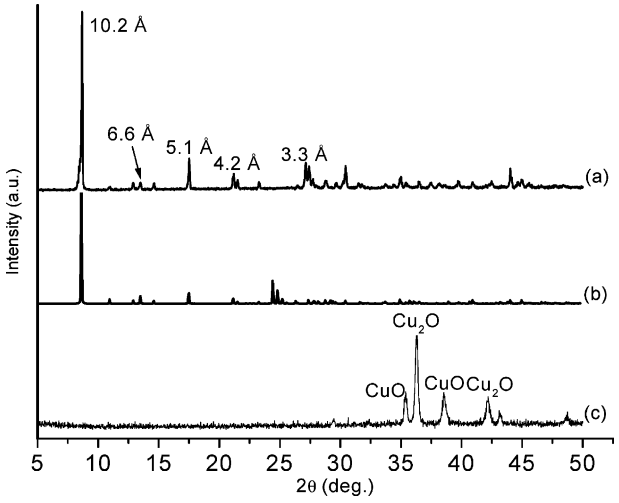

Figure 2. PXRD patterns, with most intense peaks labeled, (a) of as-synthesized material, (b) theoretical pattern project from single-crystal XRD data, (c) after treating at 600 °C.

Table 1. Crystal Data and Structure Refinement Parameters for Cu(OH)(*p*-PyC)·H_2O[a]

empirical formula	$C_6H_7CuNO_4$
T	294(2) K
cryst syst	monoclinic
space group	$P2_1/n$
unit cell dimens	$a = 3.5521(2)$ Å
	$b = 15.8665(11)$ Å
	$c = 12.9977(9)$ Å
	$\beta = 95.285(2)°$
V	729.43(7) Å^3
fw	220.67 amu
F(000)	444 ē
Z	4
density, ρ_{calcd}	2.009 g/cm^3
cryst size	0.27 × 0.09 × 0.06 mm^3
cryst color and habit	blue needle
abs coeff, μ	2.963 mm^{-1}
diffractometer	Bruker SmartApex CCD area detector
index ranges	$-4 \le h \le 4$, $0 \le k \le 21$, $0 \le l \le 17$
reflns collected	14 771 (2939 overlapped)
independent reflns	1802
obsd reflns, $I > 2\sigma(I)$	1457
coverage of independent reflns	97.8%
abs corr	semiempirical from equivalents TWINABS (Sheldrick, 1996)
max and min transmission	0.837 and 0.547
goodness-of-fit on F^2	0.927
final *R* indices	
R1, $I > 2\sigma(I)$	0.0405
wR2, all data	0.0950
R_{int}	0.0560
R_{sig}	0.0593
weighting scheme	$w = 1/[\sigma^2(F_o^2) + (0.05P)^2]$, $P = [\max(F_o^2,0) + 2F_o^2]/3$
largest diff. peak and hole	0.342 and −0.308 ē/Å^3

[a] $R1 = \Sigma||F_o| - |F_c||/\Sigma|F_o|$, $wR2 = [\Sigma w(F_o^2 - F_c^2)^2/\Sigma w(F_o^2)^2]^{1/2}$.

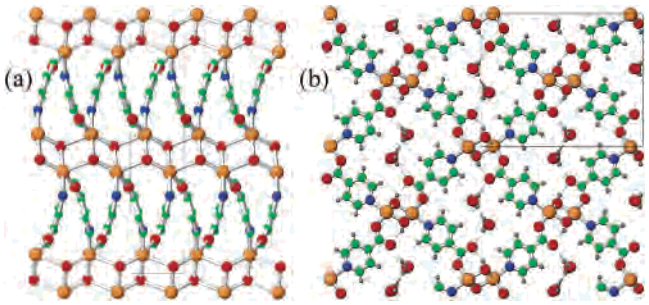

Figure 3. Crystallographic views (Cu, orange; O, red; N, blue; C, green; H, gray): (a) *c*-projection, showing the zigzag Cu(OH) chains; (b) *a*-projection of the 3D open framework with water molecules in the channels (H-bonds: thin dashed lines).

of 2.267(2) Å, typical for Cu^{2+} coordination. The shortest Cu−O bond is 1.936(2) Å and lies perpendicular to the length of the chain. The other intrachain Cu−O bond of 1.971(2) Å alternates with the substantially longer Cu−O bond length, along both edges of the zigzag chain, likely due to a Jahn−Teller distortion.[24] As a result, the Cu−Cu distances also alternate along the chain [2.965(2) and 3.107(2) Å].

The chains of edge-sharing CuO_4N distorted square pyramids are linked into a 3D framework by bridging *p*-PyC ligands (Figure 3b). The water molecule occupies the unidimensional channel and is disordered between two positions, in a 0.53 to 0.47 ratio. An extended H-bonding

(24) Yi, L.; Zhu, L.-N.; Ding, B.; Cheng, P.; Liao, D.-Z.; Zhai, Y.-P.; Yan, S.-P.; Jiang, J.-H. *Transition Met. Chem.* **2004**, *29*, 200−204.

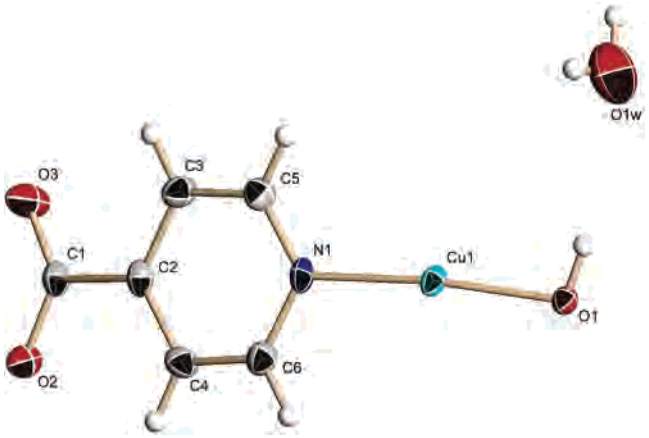

Figure 4. ORTEP diagram and atom-labeling scheme.

Table 2. Bond Lengths (Å) and Angles (deg) for Cu(OH)(*p*-PyC)·H_2O[a]

Cu1−O1	1.9358(16)	O1−Cu1−O1^{i}	81.22(7)
Cu1−O1^{i}	1.9705(17)	O1−Cu1−N1	172.07(7)
Cu1−N1	1.9931(19)	O1^{i}−Cu1−N1	91.21(7)
Cu1−O2^{ii}	2.0036(16)	O1−Cu1−O2^{ii}	95.43(7)
Cu1−O1^{iii}	2.2671(18)	O1^{i}−Cu1−O2^{ii}	153.47(8)
		N1−Cu1−O2^{ii}	92.40(7)
		O1−Cu1−O1^{iii}	85.00(7)
Cu1−Cu1^{i}	2.9654(6)	O1^{i}−Cu1−O1^{iii}	113.73(7)
		N1−Cu1−O1^{iii}	95.99(7)
		O2^{ii}−Cu1−O1^{iii}	92.02(7)
Cu1−O1−Cu1^{i}	98.78(7)	Cu1−O1−H1	105(2)
Cu1−O1−Cu1^{iii}	95.00(7)	Cu1^{i}−O1−H1	125(2)
Cu1^{i}−O1−Cu1^{iii}	113.73(7)	Cu1^{iii}−O1−H1	113(2)

[a] Symmetry transformation codes: (i) $-x+1, -y+1, -z+1$; (ii) $x-1/2, -y+3/2, z+1/2$; (iii) $-x, -y+1, -z+1$.

Table 3. Hydrogen-Bond Information[a] for Cu(OH)(*p*-PyC)·H_2O (Å and deg)

D−H···A	δ(D−H)	δ(H···A)	δ(D···A)	∠(DHA)
O1−H1···O3^{ii}	0.841(10)	1.910(18)	2.687(2)	153(3)
O2W−H2W1···O3^{ii}	0.85(2)	2.06(3)	2.892(12)	166(7)
O1W−H1W1···O1W^{iv}	0.86(2)	2.35(4)	3.20(2)	169(10)
O1W−H1W2···O3^{ii}	0.854(19)	2.59(11)	2.782(10)	94(7)

[a] D, donor atom; H, hydrogen; A, acceptor. Symmetry transformation codes:(ii) $x-1/2, -y+3/2, z+1/2$; (iv) $-x+1, -y+1, -z+2$.

network is formed between these waters and the terminal carboxylate oxygen (thin lines, Figure 3b; also see Table 3). The hydroxyl group also forms a strong intraframework H-bond with the terminal carboxylate oxygen. Batten et al.[25a,b] and Zhou et al.[25c] also used *p*-PyC as a ligand, but their structures are molecular solids ("0D"). Our compound has the unique structural feature of entirely inorganic 1D Cu(OH) chains, which are connected by organic groups into an open 3D framework. Figure 4 shows the thermal ellipsoids and atom-labeling scheme.

Magnetic Properties. Since the MOF compound contains intact 1D copper oxide chains, we investigated its magnetic properties by SQUID magnetometry. Approximately 71 mg of sample was packed between two cotton plugs and placed into a gelatin capsule. Figure 5 shows the temperature

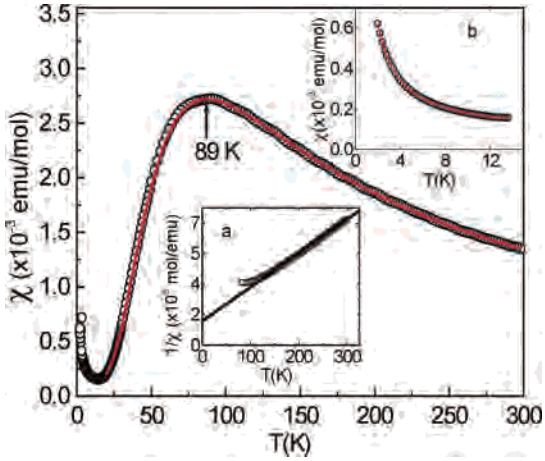

Figure 5. Temperature dependence of the susceptibility under field-cooling condition and a magnetic field of 1000 G. The solid red line is the best fit from the Heisenberg chain model (see text). Inset a shows $1/\chi$ versus temperature, while inset b shows the low-temperature region and fitting to the Curie−Weiss law.

dependence of the magnetic susceptibility, χ, between 2 and 300 K under field-cooling condition and an applied magnetic field of 1000 G (SQUID Magnetometer: Quantum Design MPMS). The susceptibility χ smoothly increases as the temperature decreases from 300 K with a broad maximum centered at 89 K that is generally associated with 1D antiferromagnetic correlations within the cuprate chains.[26] The Néel temperature T_N is around 51 K, defined by the maximum of $d(\chi T)/dT$, according to the standard definition.[27]

Figure 5a shows that the reciprocal of susceptibility deviates from linearity around 150 K. Data were fit to the modified Curie−Weiss law [$\chi = \chi_0 + C/(T - \vartheta_p)$], where χ_0 is the temperature-independent term and C is the Curie constant. We found that allowing all three parameters to vary upon data fitting gave unrealistically high values for the Curie constant and consequently g factor (2.29) in a Cu(II) system. Instead, we fixed the g factor to 2.00 and obtained a Curie constant of $C = 0.375$ emu·K/mol·Oe from the equation $C = N\mu_B^2 g^2 S(S+1)/3k_B$. In the 200−300 K region the fitting gives a paramagnetic Curie temperature ϑ_p of −33.4 K and a temperature-independent term χ_0 of 2.27×10^{-4} emu/mol·Oe. The negative value of ϑ_p indicates antiferromagnetic interaction between Cu^{2+} sites within the cuprate chain.

The data were also analyzed using the Heisenberg linear-chain theory to obtain the coupling constant J between Cu^{2+} ions in 1D spin chains.[21] The magnetic data fit very well to the Heisenberg 1D antiferromagnetic chain model[22] in the temperature range 25−300 K. The analytical expression is $\chi_{chain} = (Ng^2\mu_B^2/k_BT)(A + Bx + Cx^2)/(1 + Dx + Ex^2 + Fx^3)$, where $x = |J|/(k_BT)$ and $A-F$ are a set of coefficients required to obtain precise fits.[21c] The best fit gives parameters $J = -7.3$ cm^{-1} and $g = 2.15$, as indicated by the solid line in Figure 5. This g factor agrees well with those of related copper chain systems.[21d,28] The coupling constant $J = -7.3$

(25) (a) Batten, S. R.; Harris, A. R. *Acta Crystallogr*. **2001**, *E57*, m7−m8. (b) Batten, S. R.; Harris, A. R. *Acta Crystallogr*. **2001**, *E57*, m9−m11. (c) Zhou, Y.; Bi, W.; Li, X.; Chen, J.; Cao, R.; Hong, M. *Acta Crystallogr*. **2003**, *E59*, m356−m358.

(26) Brener, R.; Ehrenfreund, E.; Shechter, H.; Makovsky, J. *J. Phys. Chem. Solids* **1977**, *38*, 1023−1029.

(27) Fisher, M. E. *Philos. Mag*. **1962**, *7*, 1731−1734.

(28) Estes, W. E.; Gavel, D. P.; Hatfield, W. E.; Hodgson, D. J. *Inorg. Chem*. **1978**, *17*, 1415−1421.

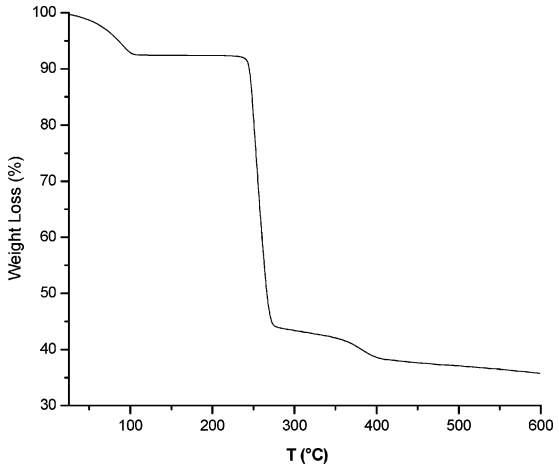

Figure 6. TGA trace of **1** shows a sharp weight loss in the 250 °C region.

cm^{-1} indicates antiferromagnetic interaction between copper ions within the chain and is consistent with the range of exchange coupling mentioned in the Introduction for the halide-bridged copper chain system.[21d]

The rapid upturn of susceptibility below 14 K indicates the presence of a small amount of paramagnetic impurity, a common occurrence in such systems and is known as a Curie tail.[29,30] This Curie tail at $kT/|J| \leq 1.25$ has been analyzed by assuming the impurity obeys the Curie law $\chi = \{P[Ng^2\mu_B{}^2S(S+1)]/3k_BT + (1-P)\chi_{chain}\}$,[28,29] where $S = 1/2$ and P is the impurity concentration. The least-squares fitting results are shown as the solid red line in Figure 5b. The resultant values of χ_0, ϑ_p, and P are 7.28×10^{-5} emu/mol·Oe, 0.08 K, and 0.2%, respectively. The impurity concentration $P = 0.2\%$ indicates the synthesized compound **1** is highly pure, as indicated by the theoretical versus experimental PXRD patterns.

Thermal Behavior. Thermogravimetric analysis shows that the material is stable to ca. 245 °C (Figure 6). The trace shows two major events. The first mass loss of ca. 7.7% occurs in the region of 50−100 °C, corresponding to the loss of intrachannel water (theoretical value 8.1%). After heating the material to 200 °C to ensure all the water is completely removed, the sample returns to approximately the same mass upon exposure to laboratory air for several hours (ca. 8.0%). PXRD analysis for the rehydrated material matches that of the as-synthesized material. A large, very abrupt mass loss of 48.5% in the 250 °C region is due to the decomposition of the *p*-PyC ligands and agrees reasonably well with the theoretical value of 55.3%.[31] The PXRD patterns after heating the material to 300, 450, and 600 °C display the same pattern (Figure 2c). The peaks of the pattern index well to Cu_2O and CuO (JCPDS refs. 05-0667 and 44−0706, respectively).

Conclusions

Extended 1D metalate chains as building blocks in metal−organic materials may lead to new materials with interesting magnetic and electrical behavior as well as small molecule storage materials. The dehydration of the material is highly reversible upon cooling from 200 °C. Preliminary studies indicate the framework is a 1D antiferromagnetic system with a Néel temperature of 51 K. The Bonner−Fisher spin chain model accounts for the magnetic behavior at $T > 25$ K, with the parameters $J = -7.3$ cm^{-1} and $g = 2.15$. A paramagnetic impurity dominates the susceptibility below 14 K and is calculated to be at a concentration of ∼0.2%, implying the synthesized compound is highly pure. Although most current focus has been on larger and more elaborate linkers, there is still a great deal of structural diversity to be explored using smaller, multidentate ligands.

Acknowledgment. This research was supported by an NSF Career Award (DMR-0239607). We also thank Professor Suzuki (SUNY Binghamton, Department of Physics) for assistance with SQUID data collection.

Supporting Information Available: Crystallographic information file (CIF) and detailed tables of atomic coordinates, anisotropic thermal parameters, and complete bond lengths and angles. This material is available free of charge via the Internet at http://pubs.acs.org.

IC050024C

(29) Rentschler, E.; Gatteschi, D.; Cornia, A. *Inorg. Chem.* **1996**, *35*, 4427−4431.

(30) Mazurek, W.; Kennedy, B. J.; Murray, K. S.; O'Connor, M. J.; Rodgers, J. R.; Snow, M. R.; Wedd, A. G.; Zwack, P. R. *Inorg. Chem.* **1985**, *24*, 3258−3264.

(31) The lower than expected mass loss is likely due to incomplete burning of the ligand in the nitrogen environment of the heating chamber.